Food Chemistry: X 23 (2024) 101673

Contents lists available at ScienceDirect

Food Chemistry: X

journal homepage: www.sciencedirect.com/journal/food-chemistry-x

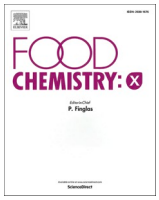

# Quantitative modelling of Plato and total flavonoids in Qingke wort at mashing and boiling stages based on FT-IR combined with deep learning and chemometrics

Xuyan Zong [a,b,1], Xianjiang Zhou [a,b,1], Xinyue Cao [a,b], Shun Gao [a,b], Dongyang Zhang [a,b], Haoran Zhang [a,b], Ran Qiu [c], Yi Wang [d], Jianhang Wu [a,b,*], Li Li [a,b,*]

[a] Liquor Brewing Biotechnology and Application Key Laboratory of Sichuan Province, Sichuan University of Science and Engineering, Yibin, 644000, Sichuan, China
[b] College of Bioengineering, Sichuan University of Science and Engineering, Yibin, 644000, Sichuan, China
[c] China Resources Snow Breweries Co., Ltd, Beijing, 100000, China
[d] Wuliangye Group Co., Ltd, Yibin, 644000, Sichuan, China

ARTICLE INFO

*Keywords:*
Craft beer
FT-IR spectroscopy
CNN
LSTM
Chemometrics

ABSTRACT

Craft beer brewers need to learn process control strategies from traditional industrial production to ensure the consistent quality of the finished product. In this study, FT-IR combined with deep learning was used for the first time to model and analyze the Plato degree and total flavonoid content of Qingke beer during the mashing and boiling stages and to compare the effectiveness with traditional chemometrics methods. Two deep learning neural networks were designed, the effect of variable input methods on the effectiveness of the models was discussed. The experimental results showed that the CARS-LSTM model had the best predictive performance, not only as the best quantitative model for Plato in the mashing ($R^2p = 0.9368$) and boiling ($R^2p = 0.9398$) phases but also as the best model for TFC in the boiling phase ($R^2p = 0.9154$). This study demonstrates the great potential of deep learning and provides a new approach to quality control analysis in beer brewing.

## 1. Introduction

Beer is now the most consumed alcoholic beverage in the world, and its brewing origins can be traced back thousands of years before Christ (Tirado-Kulieva, Hernandez-Martinez, Minchan-Velayarce, Pasapera-Campos, & Luque-Vilca, 2023). Traditionally, beer is brewed with malt, hops, water, and yeast, but traditional industrialized mass production can lead to monotonous flavors and homogenization of the market. To avoid this problem, as interest in craft beer has grown over the past few decades, brewers have begun to develop better quality and more diverse styles of craft beer, and consumption has grown faster than traditional mass-produced beers. (Coulibaly, Tohoyessou, Konan, & Dje, 2023). Different brewing ingredients can give beer different flavors; Qingke is a kind of hull-less dryland barley widely cultivated in China's high-altitude areas (Y. Zhao et al., 2024). Studies have shown that brewing Qingke as an adjunct can reduce the turbidity and color of beer, enhance the antioxidant capacity of beer, and effectively improve the foam and mouthfeel of beer (Zong et al., 2023). However, the excellent quality of the finished beer is not enough to be the key to its popularity in the market, and craft beer producers need to learn process control strategies from the large-scale brewing industry in order to maintain consistent production quality and safety standards (França, Grassi, Pimentel, & Amigo, 2021).

One of the challenges facing beer brewing over the last 50 years has been to control the quality of the malt and wort so as to obtain a high-quality finished beer, the quality of the wort has a direct impact on the quality of the finished beer, and they are pretty closely intertwined (Yin Tan, Li, Devkota, Attenborough, & Dhital, 2023). The first test for wort quality is the total dissolved malt constituents, usually expressed as Plato (°P). Adjustment of the mash by measuring real-time wort content, which facilitates future mashing control (Fox, 2020). In addition to this, antioxidant power has always been a critical parameter to be measured

* Corresponding authors at: College of Bioengineering, Sichuan University of Science and Engineering, Yibin 644000, Sichuan, China.
*E-mail addresses:* zongxuyan@suse.edu.cn (X. Zong), 322086002318@stu.suse.edu.cn (X. Zhou), 323086002201@stu.suse.edu.cn (X. Cao), 323086002207@stu.suse.edu.cn (S. Gao), 323086002227@stu.suse.edu.cn (D. Zhang), 323086002228@stu.suse.edu.cn (H. Zhang), wujianhang1996@163.com (J. Wu), lili@suse.edu.cn (L. Li).
[1] These authors contributed to the work equally and should be regarded as co-first authors

https://doi.org/10.1016/j.fochx.2024.101673
Received 26 May 2024; Received in revised form 29 June 2024; Accepted 17 July 2024
Available online 18 July 2024

during the beer brewing process in order to slow down the aging of the beer (Nardini & Garaguso, 2020). Flavonoids, due to their potent antioxidant capacity and ability to scavenge some oxidizing free radicals, also greatly influence the antioxidant power of the wort, and studies have shown that beers with more antioxidant activity are becoming increasingly popular with consumers and brewers alike (Aquilani, Laureti, Poponi, & Secondi, 2015). Monitoring the quality of the beer brewing process has always been a challenge for the industry, as it requires a range of costs, such as expensive instruments and experienced technicians (Anderson, Santos, Hildenbrand, & Schug, 2019). Another problem is the limitations of the existing monitoring techniques. In addition to conventional parameters such as temperature and pH, other indicators such as yeast vigor and antioxidant power are difficult to measure directly, as these parameters, which are derived from several related variables, interact with each other to influence the complex biological process of brewing (Kourti, 2006). As a result, some craft brewers who produce small batches can hardly afford these high costs, and the industry needs a reliable, fast, and low-cost quality assessment method to meet production needs.

Spectroscopy, as an analytical technique, is characterized by high efficiency, low cost, and non-destructive testing, which, to a certain extent, meets the inspection needs of manufacturers. Near-infrared spectroscopy (NIR) uses radiation spectra in the range of 800–2500 nm (12,500–4000 $cm^{-1}$) corresponding to overtones and combinatorial bands derived mainly from vibrational leaps of -OH, -CH, and -NH groups (Tian et al., 2023). It is capable of detecting different types of absorption by emitting multiple wavelengths to determine the nature of the sample (Helfer et al., 2022). Methods based on infrared spectroscopy have been widely used to develop reliable analytical-qualitative (pattern recognition) and quantitative (multivariate calibration) analyses of food products. Therefore, multivariate statistical analysis was used to extract useful information from NIR spectra. This helps to resolve the complex interactions between the components of the brewing process (Nobari Moghaddam, Tamiji, Akbari Lakeh, Khoshayand, & Haji Mahmoodi, 2022). Chemometrics combined with NIR plays a vital role in determining food quality. Commonly used methods for chemical composition prediction include PLSR (Partial Least Squares Regression), SVMR (Support Vector Machine Regression), ANN (Artificial Neural Network), etc. (Yan, Liu, Li, & Wang, 2023). Deep learning algorithms have made great progress in different research areas in recent years, and some researchers have proposed spectral analysis methods based on deep learning because deep learning can capture more local spectral features hidden in the original spectra (Rong, Wang, Ying, Zhang, & Zhang, 2020). For example, Convolutional Neural Networks (CNNs) can reduce the noise in the dataset during training, enabling training on smaller weights and thus reducing data complexity (Nallan Chakravartula, Moscetti, Bedini, Nardella, & Massantini, 2022). LSTM (Long Short-Term Memory) is a variant model of recurrent neural networks. The memory cells in the LSTM model are able to store the valid information from the previous wave, pass it on to the next wave, and finally synthesize all the valid information to build an analytical model of NIRS (Fu, Yang, & Wang, 2021). Valentina Giovenzana, Ana Carolina da Costa Fulgêncio (machine learning), Fujia Dong, and Shui Yu (deep learning) used NIR in combination with chemometrics or deep learning to quantitatively analyze beer-related metrics with good results (Giovenzana, Beghi, & Guidetti, 2014) (Fulgêncio, Resende, Teixeira, Botelho, & Sena, 2023) (Dong et al., 2024) (Yu, Huan, Liu, Wang, & Cao, 2023). However, the application of the methodological strategy of spectroscopy combined with chemometrics in the field of beer is mostly focused on the testing of raw materials (malt) and finished beer, and the analytical research for the brewing process is still limited.

Therefore, in this study, the methodological strategy of FT-IR (Fourier transform near-infrared) combined with chemometrics and deep learning was used to quantitatively analyze the changes in Plato and total flavonoids content (TFC) of the wort during the Qingke beer brewing process. In order to obtain a sufficiently large number of representative samples and to expand the sample range, the experiment was designed with three different mashing processes and the changes in Plato and TFC during the brewing process were analyzed. Each step of the modelling process is elaborated in detail, and the quantitative modelling effects of machine learning methods and deep learning methods are compared and discussed with a view to achieving accurate prediction of their contents so as to regulate the brewing process in a timely and relevant manner. This study can provide guidelines for quality control in the brewing process of craft beer.

## 2. Materials and methods

### 2.1. Materials

The Qingke malt for beer brewing was purchased from Ganzi Agricultural Science Institute, and the hops were purchased from East China Brewing Materials Co. Chemical analysis using ethanol, aluminum nitrate, sodium hydroxide were purchased from Kelong Chemical Co., Ltd., Chengdu, CN; Rutin standard reagent and sodium nitrite were purchased from Aladdin Biochemical Technology Co., Ltd., Shanghai, CN. All of the above are analytical grade test drugs.

### 2.2. Brewing process

For the preparation of wort, choose a 1:5 material water ratio, that is, 2 kg of Qingke malt add 10 L 35 °C hot water, 2 kg of Qingke malt and 10 L of 35 °C hot water mixing to start mashing. In order to widen the distribution of the samples and to improve the robustness of the model, this experiment used three crushing processes for Qingke malt: (a) Milling of malt to the extent of hull separation and then mashing, all using traditional processes. (b) 1 kg of Qingke malt is powdered, and the remaining 1 kg of malt is milled using traditional techniques until the hulls are separated and the two parts are mixed for mashing. (c) Use an electric grinder to powder all the Qingke malt for mashing. The temperature of the protein resting phase was set at 50 °C for 50 min; the temperature of the sugar resting phase was set at 65 °C for 90 min, which was nearly 30 min more than the conventional time, in order to explore the changes of the relevant indexes of over mashing and to facilitate the prediction of mashing endpoints through the model. At the end of mashing, the clarified wort was obtained by filtration, and the temperature was raised until the wort boiled. Hops were added in the amount of 2 g/L and boiled for 70 min. In order to obtain a sufficient number of samples, four batches of each of the three pulverization processes were repeated, and a total of 12 batches of data were obtained. The sampling time points and the number of samples are shown in Table 1, the experiment yielded a total of 228 samples in the mashing stage and 96 samples in the boiling stage, and the experimental flow of this study is shown in Fig. 1.

### 2.3. Chemical analysis methods

Plato was measured using a refractometer to take the average of three measurements of the Plato of wort samples at the same moment in time. The method of Zong et al. was used for the determination of TFC, i.e., 2.4 mL of the sample solution to be tested was mixed with 0.3 mL of 0.05 g/mL sodium nitrite solution and left to stand for 6 min; after 6 min, 0.3 mL of 0.10 g/mL aluminum nitrate solution was added, and then mixed and left to stand for 5 min; after 5 min, 4 mL of 0.04 g/mL sodium hydroxide solution was added, and then, after the reaction solution was well mixed for 15 min, the absorbance was measured at the wavelength of 510 nm. The absorbance was measured at 510 nm. The total flavonoid content was calculated from the rutin standard curve (Zong et al., 2023).

### 2.4. FT-IR spectrometer parameter settings

Near-infrared spectra of wort were collected using a Fourier

**Table 1**
Results of wort Plato changes based on three mashing processes.

| Step | Sampling temperature and time | Process (a) | | Process (b) | | Process (c) | |
|---|---|---|---|---|---|---|---|
| | | Mean (°P) | SD (°P) | Mean (°P) | SD (°P) | Mean (°P) | SD (°P) |
| Mashing | 50 °C-0 min | 2.41 | 0.2861 | 3.1425 | 0.4913 | 3.3 | 0.7765 |
| | 50 °C-10 min | 2.6825 | 0.3584 | 3.46 | 0.6367 | 3.515 | 0.8272 |
| | 50 °C-20 min | 3.0925 | 0.2206 | 4.0825 | 0.7214 | 3.85 | 0.8083 |
| | 50 °C-30 min | 3.5675 | 0.4250 | 4.6075 | 0.5511 | 4.4075 | 0.7610 |
| | 50 °C-40 min | 3.915 | 0.3335 | 4.7575 | 0.5431 | 4.5825 | 0.9738 |
| | 50 °C-50 min | 4.235 | 0.3496 | 5.0225 | 0.6043 | 4.7325 | 1.0612 |
| | 65 °C-0 min | 5.785 | 0.3539 | 8.5075 | 0.4179 | 11.365 | 1.0371 |
| | 65 °C-5 min | 6.285 | 0.3718 | 8.9675 | 0.3010 | 12.1175 | 0.9914 |
| | 65 °C-10 min | 6.5475 | 0.3285 | 9.365 | 0.3601 | 12.625 | 0.9748 |
| | 65 °C-15 min | 6.7975 | 0.3357 | 9.5425 | 0.2948 | 12.935 | 0.9809 |
| | 65 °C-20 min | 7 | 0.2376 | 9.7575 | 0.3097 | 13.15 | 1.0756 |
| | 65 °C-25 min | 7.2475 | 0.2010 | 9.965 | 0.1680 | 13.4675 | 1.1688 |
| | 65 °C-30 min | 7.3675 | 0.3060 | 10.1675 | 0.3326 | 13.4675 | 1.1001 |
| | 65 °C-40 min | 7.6325 | 0.3408 | 10.4075 | 0.3882 | 13.8025 | 1.2032 |
| | 65 °C-50 min | 7.8925 | 0.2648 | 10.6225 | 0.2986 | 13.985 | 1.1791 |
| | 65 °C-60 min | 8.1825 | 0.1842 | 10.885 | 0.2413 | 14.1 | 1.1545 |
| | 65 °C-70 min | 8.4175 | 0.2189 | 10.9175 | 0.1429 | 14.0325 | 1.1594 |
| | 65 °C-80 min | 8.5675 | 0.2421 | 10.9825 | 0.0968 | 14.235 | 1.1512 |
| | 65 °C-90 min | 8.785 | 0.3093 | 11.0675 | 0.0817 | 14.1975 | 1.1818 |
| Boiling | 0 min | 7.715 | 0.5072 | 10.565 | 0.9065 | 11.15 | 0.3405 |
| | 10 min | 8.1175 | 0.7348 | 10.9925 | 1.1288 | 11.6675 | 0.2714 |
| | 20 min | 8.605 | 0.6139 | 11.55 | 0.9571 | 12.3175 | 0.1699 |
| | 30 min | 9.215 | 0.8026 | 11.885 | 0.7428 | 12.835 | 0.3290 |
| | 40 min | 9.7175 | 0.7327 | 12.2425 | 0.8840 | 13.2725 | 0.3646 |
| | 50 min | 10.05 | 0.5723 | 12.6325 | 1.0189 | 14.25 | 0.4785 |
| | 60 min | 10.4 | 0.5224 | 13.1075 | 1.1807 | 14.7 | 0.3673 |
| | 70 min | 11.0975 | 0.6717 | 13.6 | 0.9957 | 15.3 | 0.4504 |

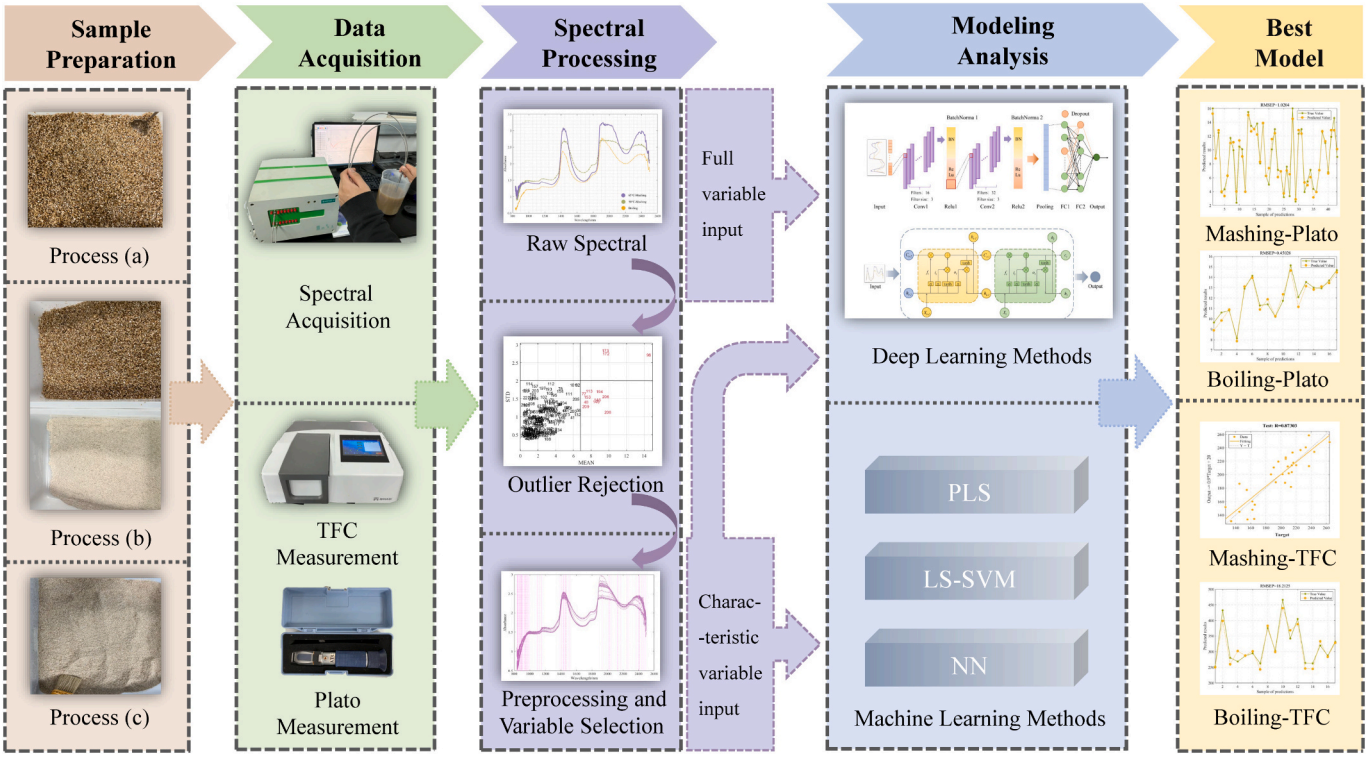


**Fig. 1.** Experimental procedure overview.

transform near-infrared spectrometer (Insa Optics, Shanghai, China), model master 10. In order to collect the spectra of the samples in real-time, it is necessary to put the spectral collector directly into the samples to collect the spectral information and then take into account the high-temperature environmental characteristics of the experiment so the immersion-type fiber optic probe is used for the spectral collection of the wort. When analyzing liquid samples, spectrometers often use the transmission-reflection mode; when the liquid under test enters the cavity at the front end of the probe, the light shines into the liquid from the incident light path, reflects off the reflector and returns to the liquid and then enters the reflected light path, and finally enters the spectrometer for spectral determination. Therefore, the measurement

method was selected to be transreflective, the wavelength range was from 12,000 $cm^{-1}$ to 4000 $cm^{-1}$, the resolution was set to 8 $cm^{-1}$, and the detector was DLATGS.

### 2.5. Chemometrics methods

#### 2.5.1. Outlier rejection

The appearance of outliers will increase the error of the experimental data, thus affecting the regression, which ultimately leads to poor training of the whole model. The elimination of outlier samples can effectively improve the model's robustness, generalization, and prediction ability. In this experiment, the predetermined number of cycles is set to 1000. The sample set is divided into training and validation sets in the ratio of 8:2. Then, MCCV (Monte Carlo Cross Validation) is used to calculate the outliers in the sample dataset (Xuan et al., 2023).

#### 2.5.2. Preprocessing

Preprocessing the raw spectra removes unwanted or negatively impacted signals from the spectral data, and appropriate preprocessing methods are beneficial to modelling (Jiao, Li, Chen, & Fei, 2020). Smoothing correction can reduce the noise of the spectrum and improve the signal-to-noise ratio; scattering correction methods such as SNV and MSC can eliminate the scattering effect due to the uneven size and distribution of the sample particles; operations such as DE1 and DE2 derivation can remove unimportant baseline signals, smooth the impact of the background interference, and improve the higher resolution. All these methods can improve the data quality to a certain extent. In this experiment, preprocessing methods such as SM (Smoothing), DE1 (First-order Derivative), DE2 (Second-order Derivative), MSC (Multiplicative Scatter Correction), SNV (Standard Normal Variate), and a two-by-two combination of derivation and scattering correction algorithms (DE1 + MSC, DE2 + MSC, DE1 + SNV, DE2 + SNV) are used to preprocess the FT-IR spectra. The optimal preprocessing method was finally determined by $R^2$ and RMSECV (Root Mean Square Error of Cross Validation). They are calculated as shown below:

$$R^2 = 1 - \frac{\sum_{i=1}^{n}\left(y_{i,actual} - y_{i,predicted}\right)^2}{\sum_{i=1}^{n}\left(y_{i,actual} - \bar{y}_{actual}\right)^2} \quad (1)$$

$$RMSECV = \sqrt{\frac{\sum_{i=1}^{n}\left(y_{i,actual} - y_{i,predicted}\right)^2}{n-1}} \quad (2)$$

where $y_{i,actual}$ is the actual value of the ith sample; $y_{i,predicted}$ is the predicted value of the ith sample; $y_{actual}$ is the mean of all true values, and n is the number of samples.

#### 2.5.3. Variable selection

Full-spectrum variational models contain a large amount of redundant information, which can negatively affect model predictions. Many experiments and theories have shown that the performance of calibrated models can be improved by using selected wavelengths of information instead of the full spectrum. The CARS algorithm is currently a more widely used spectral variable selection technique in the field of spectral modelling. It draws on the genetic mechanism of nature's organisms and gradually evaluates and analyzes, screens, and eliminates each wavelength point in the spectrum, which helps to establish a robust analytical model against external factors and reduce the information redundancy and multicollinearity problems of the spectral matrix. The selection of the optimal combination of wavelengths present in the full spectrum combined with partial least squares regression can be effectively used for wavelength selection to build high-performance calibration models (H. Li, Liang, Xu, & Cao, 2009). Therefore, the CARS algorithm is used for feature wavelength selection in this experiment.

#### 2.5.4. Selection of calibration and prediction set

Commonly used sample partitioning methods include RS (Random Selection), KS (Kennard-Stone) algorithm and SPXY (Sample set partitioning based on joint x-y distance) algorithm. The KS algorithm is a classical ensemble partitioning method that selects samples that are uniformly distributed over the prediction space. KS can select samples based on spectral features and is sensitive to spectral changes after preprocessing (Liu et al., 2019). The KS algorithm is suitable for analytical chemistry applications because it allows the training model to cover most of the sources of variation in the dataset, ensuring that the training model is more representative of the entire dataset. Therefore, the KS algorithm was chosen for this experiment to partition the dataset (C. Li et al., 2022).

#### 2.5.5. Modelling regression methods

The most commonly used multivariate correction methods are PCR (Principal Component Regression) and PLS (Partial Least Squares), both of which, to some extent, overcome the limitations of MLR (Multiple Linear Regression). These methods are based on correlating the independent X-block of spectral data with the relevant Y-block of the values to be predicted through inverse calibration and then selecting the number of PCs (principal components) or LVs (latent variables) through cross-validation. Based on the principle of parsimony, the analytical chemist should choose a linear model such as PLS or orthogonal PLS. However, if the parsimonious linear model does not predict well due to the wide range of analysis, one can try to use nonlinear models such as ANN as well as SVM (Augusti et al., 2024). Least Squares Support Vector Machines are an extension of Support Vector Machines in the form of quadratic loss functions. This nonlinear modelling method replaces the complex quadratic optimization problem in Support Vector Machines by solving a set of linear equations. This method can improve the model generalization ability through the principle of structural risk minimization and has a good advantage in solving problems with small samples, nonlinearities, and high dimensions. ANN is able to simulate the structure and function of neural feedback of the human brain in a mathematical model with a high degree of self-learning, adaptation, and feedback capabilities. It has also long been widely used to deal with nonlinear problems in complex processes. In this experiment, PLS, LS-SVM and ANN are used for regression modelling.

### 2.6. Deep learning methods

#### 2.6.1. CNN

A classical CNN usually consists of several convolutional layers, an activation function layer, a pooling layer, and some fully connected layers. The main function of the convolutional layer is to extract local abstract features, while the activation function layer implements linear or nonlinear mapping. The pooling layer is usually used to reduce the dimensionality of the feature vectors in the convolutional layer. The mapping relationship between the extracted abstract features and the target output is established through the fully connected layer. Through iterative parameter tuning, CNNs are able to optimize the performance of the model by training millions of parameters and extracting relevant features of the spectral data (Banerjee, Mandal, Jesubalan, Jain, & Rathore, 2024). This study compares the effect of two input methods on the accuracy of the final prediction model. Method 1 is to use all the spectral data without any preprocessing as the input to the CNN, and method 2 is to use the feature variables screened by the CARS algorithm after processes such as outlier exclusion and after spectral preprocessing as the input to the CNN. Based on the fixed model training parameters, the network architecture of the CNN is debugged, thereby determining the optimal network structure.

#### 2.6.2. LSTM

LSTM is mainly used to solve the problem of gradient vanishing and gradient explosion in long sequence training, and its core idea is to

control the neuron states of memory tuples and nonlinear gate units. The nonlinear gate unit is used to regulate the flow of information in and out of the storage tuple at each point in time. It consists of several parts: the Sigmoid neural network layer, the Tanh activation function, and the point-by-point multiplier (Lindemann, Maschler, Sahlab, & Weyrich, 2021). Like CNN, this study also compares the effect of the two variable input methods on the accuracy of the final prediction model. It determines the optimal LSTM network structure through debugging.

#### 2.6.3. Model evaluation indicators

All models were evaluated using RMSEC (Root Mean Square Error of Calibration), RMSEP (Root Mean Square Error of Prediction), $R^2c$ (Calibration set coefficient of determination), $R^2p$ (Prediction set coefficient of determination), and RPD (Relative Percentage Deviation) values were used for the evaluation of the effect. The closer the $R^2$ is to 1, the better the predictions. Similarly, the smaller the RMSEC and RMSEP, the better the modelled regression. The RPD value was used as a criterion to judge the robustness of the model, and when the RPD value was lower than 1.5, the model was considered to be insufficiently constructed, and the samples could only be roughly analyzed quantitatively. An RPD in the range of 1.5–2.0 is considered to have the potential for the model to distinguish between high and low values, while an RPD value between 2.0 and 2.5 indicates that the model can make approximate quantitative predictions; an RPD of 2.5–3.0 and greater than 3.0 indicates that the model has good and excellent prediction results (Huang, Fan, Li, Meng, & Liu, 2022). They are calculated as shown below:

$$R^2c = 1 - \frac{\sum_{i=1}^{n}\left(y_{i,actual} - y_{i,predicted}\right)^2}{\sum_{i=1}^{n}\left(y_{i,actual} - \overline{y}_{actual}\right)^2} \tag{6}$$

$$RMSEC = \sqrt{\frac{\sum_{i=1}^{n}\left(y_{i,actual} - y_{i,predicted}\right)^2}{n-1}} \tag{7}$$

where $y_{i,actual}$ is the actual value of the ith sample of the calibration set; $y_{i,predicted}$ is the predicted value of the ith sample of the calibration set; $y_{actual}$ is the mean of all true values, and n is the number of samples in the calibration set.

$$R^2p = 1 - \frac{\sum_{k=1}^{m}\left(y_{k,actual} - y_{k,predicted}\right)^2}{\sum_{k=1}^{m}\left(y_{k,actual} - \overline{y}_{actual}\right)^2} \tag{8}$$

$$RMSEP = \sqrt{\frac{\sum_{k=1}^{m}\left(y_{k,actual} - y_{k,predicted}\right)^2}{m-1}} \tag{9}$$

where $y_{i,actual}$ is the actual value of the kth sample of the prediction set; $y_{i,predicted}$ is the predicted value of the ith sample of the prediction set; $y_{actual}$ is the mean of all true values, and m is the number of samples in the prediction set.

$$RPD = \frac{1}{\sqrt{1 - \left(R^2p\right)^2}} \tag{10}$$

### 2.7. Software and hardware

FT-IR data acquisition software: FTIRDasAnalyzer (Insa Optics, Shanghai, China); Data preprocessing, feature variable selection, and model building were performed in MATLAB R2015a (MathWorks, Natick, MA, USA). The plots of the experimental results were also plotted using MATLAB. The calibration was performed on a personal computer equipped with an Intel (R) core (TM) i5-8300H CPU at 2.3 GHz clock frequency, 16GB RAM and GPU Nvidia Geforce GTX 1050 Ti.

## 3. Results and discussion

### 3.1. NIR spectral analysis

The raw FT-IR spectra of wort at the mashing and boiling stages are shown in Fig. 2. The wavelength range of the NIR spectra of this experiment is 833–2500 nm, with very distinct absorption peaks at around 1450 nm and 1900 nm, and these characteristic absorption peaks all contain different levels of sample information. Based on previous studies on Qingke wort, the absorption peak around 1450 nm originates from the combined frequency vibration of the C—H ($CH_3$, $CH_2$) groups. The absorption peaks around 1900 nm may originate from the 1st frequency of $CH_2$, $CH_3$ and other groups. Some inconspicuous absorption peaks, such as those at 1150 nm and 2350 nm, originate from the 2nd frequency and combinatorial frequency vibrations of the C—H ($CH_3$, $CH_2$), respectively (Zhou et al., 2024). As the mashing temperature increased, the absorbance increased gradually. When the wort is at the boiling stage, the absorbance decreases. Still, the spectral curve becomes smoother because the wort system is more clarified after filtration, and the light scattering effect due to the roughness of the malt surface is reduced.

### 3.2. Chemical analysis results

The results of changes in Plato and TFC of wort during the mashing and boiling stages are shown in Table 1 and Table 2. During mashing, the activity of endogenous enzymes in the malt converts starch into fermentable sugars, digests proteins into peptides and amino acids, and releases micronutrients. The α- and β-amylases cleave the α-(1 → 4) linkages in starch, releasing mainly maltose and glucose. Both crushing and enzyme treatment significantly affects the Plato of Qingke barley wort, which is usually used for the initial assessment of wort quality and characterizes the soluble solids content of Qingke barley wort. Measurement of wort Plato can be a rough judgment of the sugar in the wort so that industrial production of the relevant process to make timely adjustments, when the wort is in the 50 °C protein rest stage, as the percentage of Qingke powder in the brewing process rises, Plato has a significant increase, the average Plato of the three processes is not much difference, and finally maintained at about 5. Plato rises substantially when warmed to 65 °C. The higher the malt crush, the higher the Plato and this result is in line with Li et al.'s study on Qingke beer, which showed that the Plato of the wort at the mashing stage usually stays around the range of 3–10 (L. Li et al., 2023). When the mashing phase was over, there was a significant difference in Plato size between the three brewing processes, with both adjacent processes having an almost 3 difference. When the wort enters the boiling stage, the volume of filtered wort is controlled to 10 L by washing the leaves and other operations. As the water evaporates, the wort is further thickened, and the Plato, which has been lowered by lees washing, rises again. When the boiling phase ended, the average Plato reached a maximum of 15.3 (process (c)).

Phenolics are mainly present in the bran and endosperm of Qingke in free or bound form, including phenolic acids and their flavonoids. In order to investigate the possible relationship between phenolics (total phenols, total tannins, total flavonoids and total anthocyanins) and antioxidant activity (antiradical activity and iron-reducing antioxidant capacity). Wahauwou'el'e Hermann Coulibaly et al. created a correlated Pearson matrix, and the results of the test showed that the anti-free radical activity was closely and positively correlated with total phenols, total flavonoids and total anthocyanins (Coulibaly et al., 2023). Thus, controlling the TFC during beer brewing can help enhance the antioxidant capacity of Qingke wort and its flavour stability. The TFC increased steadily with time when the wort was in the protein resting stage at 50 °C. The TFC was further elevated up to 240 mg/L when the elevated temperature brought the wort to the sugar resting stage. However, the TFC at this stage does not increase linearly. This is because

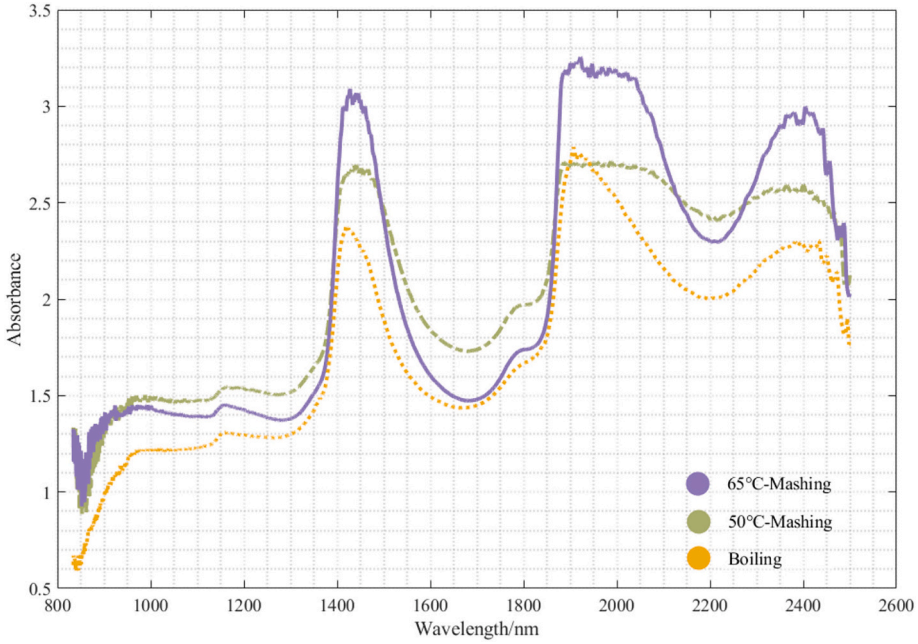


**Fig. 2.** FT-IR raw spectra of different stages of wort.

**Table 2**
Results of wort TFC changes based on three mashing processes.

| Step | Sampling temperature and time | Process (a) | | Process (b) | | Process (c) | |
|---|---|---|---|---|---|---|---|
| | | Mean (mg/L) | SD (mg/L) | Mean (mg/L) | SD (mg/L) | Mean (mg/L) | SD (mg/L) |
| Mashing | 50 °C-0 min | 150.9306 | 23.5794 | 139.0556 | 8.4827 | 158.3611 | 14.8233 |
| | 50 °C-10 min | 155.8958 | 19.2441 | 142.2847 | 11.5313 | 168.5000 | 12.3124 |
| | 50 °C-20 min | 164.8194 | 23.5479 | 141.7292 | 8.1693 | 167.0069 | 21.5740 |
| | 50 °C-30 min | 182.2153 | 20.9051 | 154.9583 | 5.7977 | 187.9444 | 20.9930 |
| | 50 °C-40 min | 181.9028 | 23.4430 | 159.4028 | 3.8125 | 181.4514 | 9.8500 |
| | 50 °C-50 min | 189.2639 | 23.0258 | 164.8194 | 7.6307 | 183.7083 | 12.5015 |
| | 65 °C-0 min | 214.5417 | 17.4462 | 193.0139 | 9.1070 | 206.1736 | 14.8053 |
| | 65 °C-5 min | 212.2500 | 8.3625 | 206.6597 | 12.3347 | 224.9931 | 7.3999 |
| | 65 °C-10 min | 205.9306 | 16.4708 | 181.1042 | 4.0234 | 196.7639 | 10.7039 |
| | 65 °C-15 min | 232.8750 | 38.4317 | 188.4306 | 4.0505 | 202.9792 | 23.4752 |
| | 65 °C-20 min | 210.4097 | 15.9536 | 193.0139 | 4.7396 | 214.8542 | 10.6063 |
| | 65 °C-25 min | 236.9028 | 34.7673 | 202.7014 | 8.9588 | 209.9931 | 7.4032 |
| | 65 °C-30 min | 220.4097 | 13.8490 | 194.1250 | 6.4145 | 211.6944 | 7.2705 |
| | 65 °C-40 min | 229.4375 | 14.5132 | 215.8958 | 21.2784 | 209.2292 | 14.0114 |
| | 65 °C-50 min | 231.7639 | 17.6878 | 211.7292 | 8.5602 | 210.8611 | 12.4654 |
| | 65 °C-60 min | 239.1944 | 13.3624 | 238.5694 | 13.0393 | 233.2222 | 9.2026 |
| | 65 °C-70 min | 229.7153 | 27.2869 | 193.2917 | 22.9988 | 217.8750 | 19.8166 |
| | 65 °C-80 min | 235.5833 | 10.0790 | 212.1806 | 17.6195 | 221.8681 | 21.1605 |
| | 65 °C-90 min | 242.7014 | 14.1122 | 212.9097 | 14.4078 | 225.4097 | 12.6889 |
| Boiling | 0 min | 289.2639 | 18.0830 | 270.4444 | 11.8612 | 246.7639 | 31.5975 |
| | 10 min | 309.2292 | 14.2415 | 290.9306 | 24.5509 | 276.1736 | 40.1861 |
| | 20 min | 332.4583 | 24.2135 | 282.8750 | 26.6636 | 279.5069 | 42.8291 |
| | 30 min | 358.3611 | 21.7390 | 312.9444 | 27.1971 | 299.7847 | 45.4894 |
| | 40 min | 372.1111 | 36.0177 | 291.1042 | 42.9431 | 307.0069 | 50.7790 |
| | 50 min | 385.0972 | 35.6262 | 317.6667 | 34.1487 | 326.9722 | 43.9979 |
| | 60 min | 399.5764 | 33.8432 | 309.6806 | 13.1531 | 360.0972 | 44.9452 |
| | 70 min | 447.2847 | 12.4565 | 359.7847 | 12.2366 | 388.1181 | 39.4187 |

mashing is not a single substance changing but a series of reactions between a series of substances (Martínez et al., 2017). When the wort was boiled at the completion of boiling, the TFC increased significantly. The TFC of the process (a) was the largest among the three processes, with an average TFC of 447.2847, which is in line with the findings that phenolics are mainly found in Qingke bran and endosperm. And It is also possible that the flavonoid content rose due to the addition of hops, which have a high flavonoid content. Similarly, as the water evaporates, the concentration of the substance increases.

### 3.3. Outlier rejection results

Fig. 3 is a plot of the results of FT-IR spectroscopy for the rejection of Plato and TFC outlier at the mashing and boiling stages, with the horizontal coordinate representing the absolute value of the mean and the vertical coordinate representing the standard deviation of the samples. Samples near the zero point were defined as normal, and other samples that deviated from this region were described as having anomalous spectral and chemical values. The effectiveness of this operation is judged based on the change in the values of $R^2$ and RMSECV before and

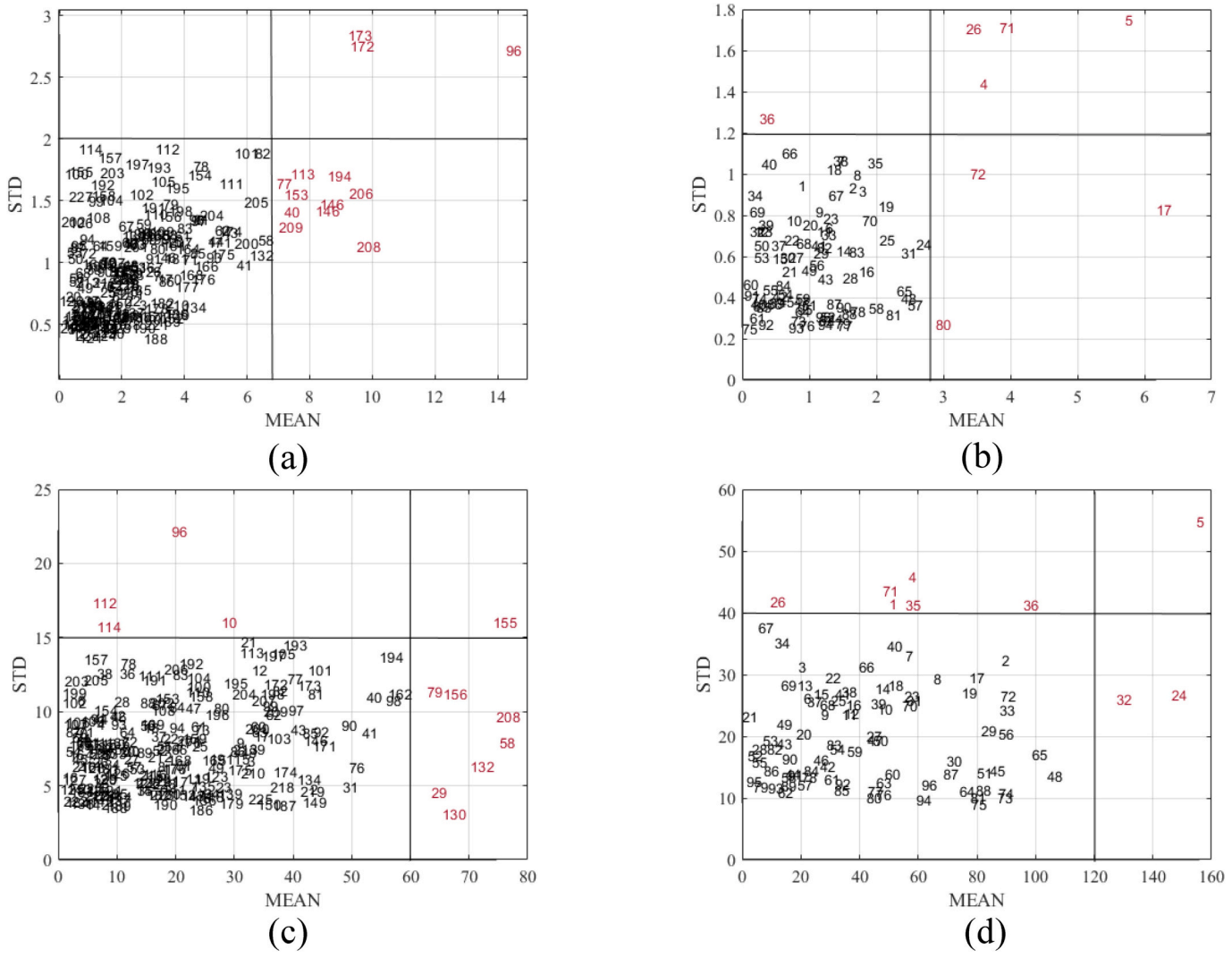


**Fig. 3.** Outlier rejection results; (a) Plato and spectral outliers in the mashing stage; (b) Plato and spectral outliers in the boiling stage; (c) TFC and spectral outliers in the mashing stage; (d) TFC and spectral outliers in the boiling stage.

after the outlier rejection operation. Specific values can be seen in Table S1, and it can be found that after the outlier removal operation, the $R^2$ of the model has a certain degree of increase. In contrast, the RMSECV has a certain degree of decrease (which represents the error between the actual value and the predicted value is reduced), which proves the validity and necessity of this operation. All these outliers need to be rejected in advance of the subsequent analysis of the model because the outliers will not only mislead the selection of spectral variables but also shift the model parameters, which will reduce the predictive accuracy of the model to some extent.

### 3.4. Spectral preprocessing results

As shown in Table S1, after processing the raw sample spectra using different preprocessing methods, the spectral data is processed by selecting the best preprocessing method for quantitative modelling. The $R^2$ and RMSECV in CARS-PLS are used to choose the best preprocessing method and feature wavelength. The closer the $R^2$ is to 1, the higher the accuracy is, and the smaller the RMSECV is, the better the model prediction is. The results show that for the spectra of Plato in the mashing stage, the preprocessing method of first-order derivatives combined with SNV achieved the best results, with an $R^2$ of 0.8424 and an RMSECV of 1.4338, and 139 feature variables were obtained after the screening of the CARS algorithm. For the spectra of Plato in the boiling phase, the same preprocessing method of first-order derivative combined with SNV achieved the best results, with an $R^2$ of 0.8699 and an RMSECV of 0.7084, and 58 feature variables were obtained by screening with the CARS algorithm. For the spectra of TFC in the mashing stage, the best results were achieved by the MSC preprocessing method, which reached an $R^2$ of 0.7826 and an RMSECV of 14.2941, and 90 feature variables were obtained after screening by the CARS algorithm. For the spectra of TFC in the boiling phase, the preprocessing method of second-order derivatives combined with SNV achieved the best results, with an $R^2$ of 0.8271 and an RMSECV of 23.2092, and 67 feature variables were obtained after the screening of the CARS algorithm.

The best preprocessing results are achieved in this part of the derivation and spectral scattering correction algorithm because the derivation calculation reduces the variability background, corrects the drifting baseline, and improves the resolution and sensitivity of the spectra (Shao, Cui, Wang, & Cai, 2019). Whereas the rough surface of the malt causes light scattering, MSC and SNV are able to eliminate the scattering effect caused by different particle sizes or uneven distribution.

### 3.5. Variable selection results

In this study, a total of 1700 wavelengths were incorporated into the full-spectrum-based prediction model, and the accuracy of the prediction model was improved after spectral preprocessing. However, there

are still problems, such as long model computation time and full-wavelength data covariance. Therefore, there is a need to address these issues by simplifying and feature-extracting the spectral data in order to increase the computational speed of the model. Fig.S7 illustrates the variable screening process for CARS. The number of times the experiment was sampled using Monte Carlo was 50. The top graph represents that as the number of samples increases, the wavelength variable decreases rapidly and then decreases slowly, i.e., the wavelength variable goes from rough screening to careful screening. The middle plot represents the process in which the root mean square error in the cross-validation set shows a slow decrease to a minimum and then a rapid increase during feature wavelength picking. As the value of RMSECV decreases gradually, it indicates that the characteristic wavelengths associated with Plato are included. When it reduces to the minimum value and then increases, it predicts that the wavelengths associated with Plato are being gradually eliminated, and the smallest RMSECV of 1.4338 is obtained. The bottom plot shows the variation of the regression coefficients of the wavelength variables, and the sampling is stopped at position * when the obtained RMSECV is the minimum, at which point the number of samples is 20. Some of the valuable variables are eliminated if the sampling is continued. So 139 characteristic wavelengths are extracted when the sampling number is 20 times, accounting for 8.17% of the total number of wavelengths.

The number of feature wavelengths obtained after screening by the CARS algorithm is recorded in Table.S1, and the distribution of feature wavelengths in the full spectrum is shown in Fig. 4. From the distribution, the feature peaks at about 900 nm, 1100 nm, 1400 nm, 1900 nm, and 2400 nm wavelengths have more feature variable distributions, and this result proves the superiority of the CARS algorithm, it is able to extract the spectral feature information effectively. However, the results of cross-validation of total flavonoids and spectra at the mashing stage using CARS were generally poor, with a non-significant change in its predictive accuracy compared to the full-wavelength prediction model, which could be attributed to the elimination of wavelengths containing critical information during the wavelength screening process, resulting in a decrease in model performance (L. Li et al., 2023).

### 3.6. *Deep learning parameter tuning results*

The structure of CNN and LSTM networks constructed in this study is shown in Fig. 5. On the basis of determining the training parameters of the network, the structure of the optimal quantitative network model

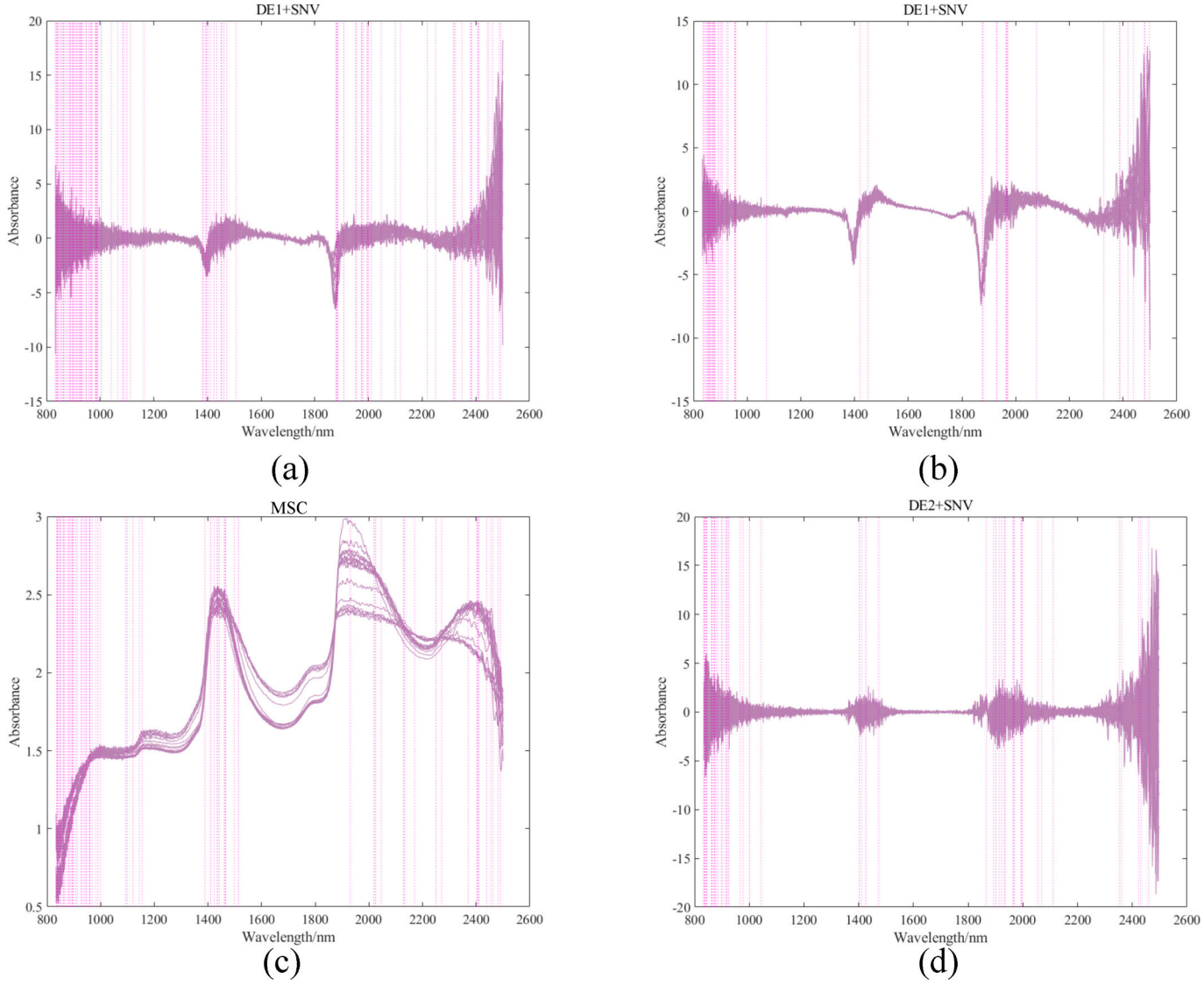


**Fig. 4.** Outlier rejection results based on optimal spectral preprocessing methods; (a) Plato and spectral variable selection results in the mashing stage; (b) Plato and spectral variable selection results in the boiling stage; (c) TFC and spectral variable selection results in the mashing stage; (d) TFC and spectral variable selection results in the boiling stage.

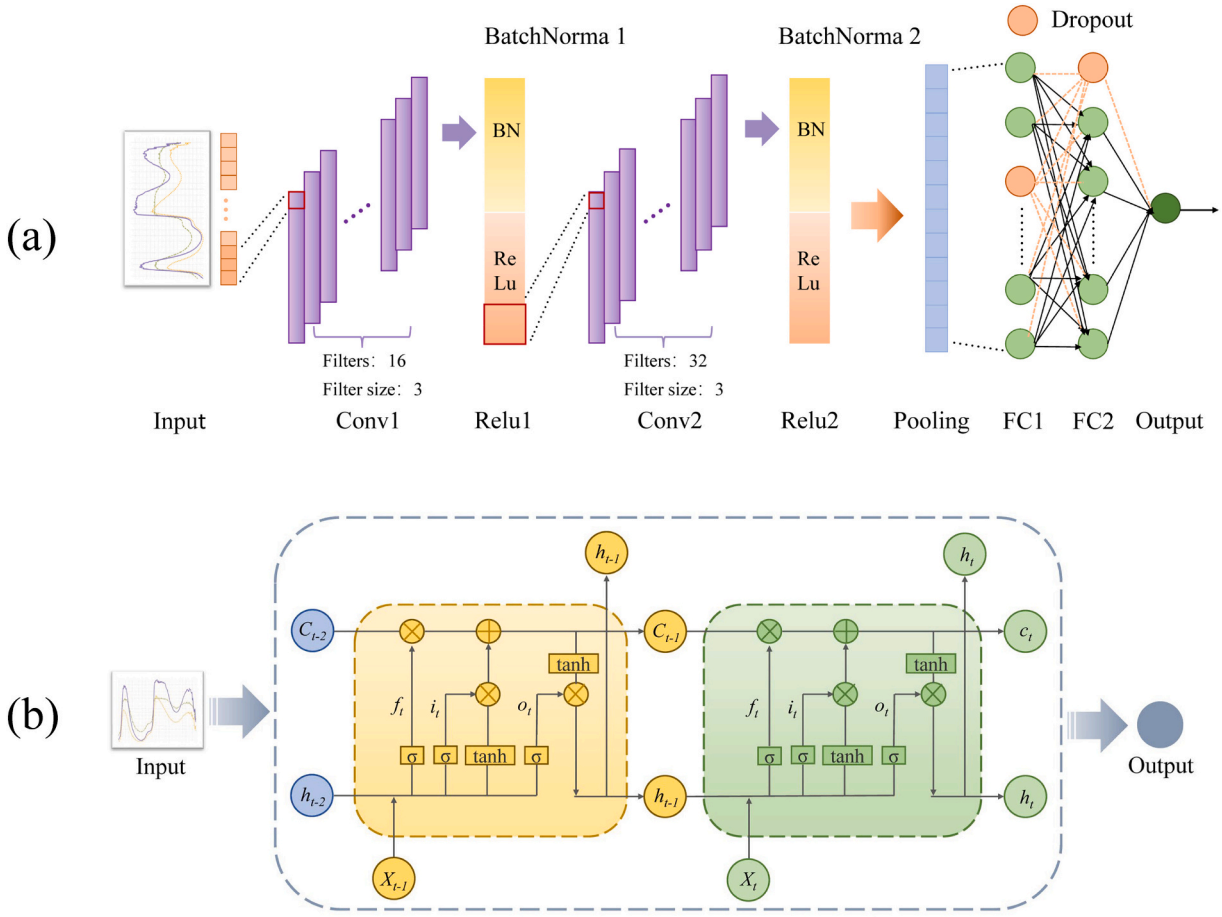


**Fig. 5.** Optimal construction of deep learning networks; (a) CNN; (b) LSTM; Conv: convolution2dLayer; BatchNorma: batchNormalizationLayer; Relu: ReluLayer; Pooling: maxPooling2dLayer; FC: fullyconnectedLayer; $X_t$: Input data from memory cells; $h_t$: Memory cell hidden layer output; $C_t$: Storing memory cell information; $C_{t-1}$ and $h_{t-1}$: Memory cell information from the previous moment and hidden layer outputs; Xt, $C_{t-1}$ and $h_{t-1}$: Input of memory cells; $f_t$: Forgetting part of the input information; $i_t$: Memorize some of the input information; $O_t$: Control output information; Tanh: activation function; σ: sigmoid activation function.

was finally determined by changing the number of convolutional layers, the size of the convolutional kernel, the size of the pooling window, the size of the training batch and other structural indicators and then iteratively training the network. The experiment was designed with two different variable inputs, one for the full wavelength of the spectrum and the other with the characteristic wavelengths screened by the CARS algorithm as inputs. It should be noted that due to the excessive number of full-wavelength wavelengths, in order to enhance the regression prediction effect of the network, the network adds two more fully-connected layers, with the number of FC1 set to 100 and the number of FC2 set to 50. In contrast, the number of FCs for the network that takes a featured-wavelength input is set to only one. In order to enhance the robustness and generalization of the model, a dropout layer is also introduced as a fully connected layer of the model training process. In addition, because the number of samples in the boiling phase (96) was considerably less than the number of samples in the saccharification phase (228), a new gradient was set for the training batch size in the boiling phase in order to train the network adequately. The training parameters of the network are shown in Table S5 and Tables S2-S4 demonstrate the process of tuning the structural parameters of the network. A certain network parameter is varied, and successive training is done to obtain eight models. In contrast, other parameters are kept unchanged, and finally, the gradient with the largest average value of $R^2p$ is determined to be the optimal structural parameter.

The final number of convolutional layers for CNN is set to 2, the convolutional kernel size is 3, the pooling window size is set to 2, and the Batch size is 50; for LSTM, the number of layers is set to 2, the number of neurons in a single layer is 20, and Batch size is 50. The batch size is set to 20 for CNN and 30 for LSTM in the boiling stage. The variation of the Loss function and RMSE values for network training is shown in Fig. S6. The training of a deep learning network model is actually the process of minimizing the loss value by continuously adjusting the difference between the predicted output and the actual output. The smaller the value of the loss function, the smaller the difference between the expected output and the actual result (desired output). Taking the Plato data in the mashing stage as an example, it can be seen that the RMSE of the CNN model decreases rapidly with the increase in the number of iterations, and after about 100 network training, its RMSE value decreases substantially. Then, the decrease slows down to convergence. The LSTM model, on the other hand, went through almost 400 iterations before the RMSE began to converge. It can be seen that both network models have better stability and generalization.

### 3.7. Quantitative prediction model results

The results of all the quantitative prediction models are shown in Table 3. For the quantitative analysis of Plato in Qingke wort, the CARS-LSTM model has the best prediction performance both in the mashing and boiling stages, with its $R^2p$ reaching more than 0.93 and its RPD reaching more than 2.8, which represents that the model has a very good prediction effect. For the quantitative analysis of TFC, ANN took the best prediction at the mashing stage ($R^2p = 0.873$, RPD = 2.0504), but this was only an approximate quantitative analysis of TFC. Similarly, CARS-LSTM achieved the best quantitative prediction of TFC in the boiling

**Table 3**
Modelling results for quantitative prediction of Plato and TFC in wort.

| Analysis object | Step | Preprocessing method | Characteristic wavelength number | Modelling Method | $R^2c$ | RMSEC | $R^2p$ | RMSEP | RPD | Time |
|---|---|---|---|---|---|---|---|---|---|---|
| Plato | Mashing | DE1-SNV | 139 | PLS | 0.9669 | 0.6583 | 0.8898 | 1.2027 | 2.1913 | |
| | | | | LS-SVM | 0.9998 | 0.0503 | 0.8391 | 1.5367 | 1.8383 | |
| | | | | ANN | 0.9957 | 0.3828 | 0.842 | 2.0392 | 1.8536 | |
| | | | | CARS-CNN | 0.9928 | 0.3056 | 0.8419 | 1.4731 | 1.8531 | 54 s |
| | | | | **CARS-LSTM** | **0.9992** | **0.0962** | **0.9368** | **1.0204** | **2.8582** | 50s |
| | | | | CNN | 0.8667 | 1.3944 | 0.7516 | 1.7199 | 1.5160 | 192 s |
| | | | | LSTM | 0.9337 | 0.9771 | 0.828 | 1.5309 | 1.7834 | 80s |
| | Boiling | DE1-SNV | 58 | PLS | 0.975 | 0.3118 | 0.8689 | 0.6956 | 2.0203 | |
| | | | | LS-SVM | 0.9995 | 0.0419 | 0.8667 | 0.8188 | 2.0047 | |
| | | | | ANN | 0.9978 | 0.1691 | 0.8669 | 0.869 | 2.0061 | |
| | | | | CARS-CNN | 0.9862 | 0.2326 | 0.8822 | 0.6217 | 2.1237 | 30s |
| | | | | **CARS-LSTM** | **0.9964** | **0.1178** | **0.9398** | **0.4503** | **2.9263** | 26 s |
| | | | | CNN | 0.7971 | 0.9608 | 0.4144 | 0.9608 | 1.0988 | 179 s |
| | | | | LSTM | 0.8266 | 0.8831 | 0.6395 | 1.0741 | 1.3007 | 42 s |
| TFC | Mashing | MSC | 90 | PLS | 0.8824 | 10.5673 | 0.6634 | 16.5451 | 1.3364 | |
| | | | | LS-SVM | 0.9792 | 4.3963 | 0.6871 | 17.2507 | 1.3763 | |
| | | | | **ANN** | **0.9655** | **8.2394** | **0.873** | **17.5415** | **2.0504** | |
| | | | | CARS-CNN | 0.8793 | 10.5723 | 0.7534 | 15.5734 | 1.5208 | 52 s |
| | | | | CARS-LSTM | 0.8969 | 9.5823 | 0.8385 | 13.5388 | 1.8352 | 48 s |
| | | | | CNN | 0.8836 | 10.6249 | 0.5855 | 22.8922 | 1.2335 | 212 s |
| | | | | LSTM | 0.8333 | 13.2318 | 0.4429 | 23.0711 | 1.1154 | 115 s |
| | Boiling | DE2-SNV | 67 | PLS | 0.9842 | 6.7002 | 0.8842 | 21.541 | 2.1408 | |
| | | | | LS-SVM | 0.999 | 1.7272 | 0.7276 | 32.654 | 1.4577 | |
| | | | | ANN | 0.9963 | 4.991 | 0.7972 | 27.8567 | 1.6564 | |
| | | | | CARS-CNN | 0.9762 | 8.376 | 0.736 | 31.7678 | 1.4771 | 30s |
| | | | | **CARS-LSTM** | **0.9991** | **1.5835** | **0.9154** | **18.2125** | **2.4842** | 28 s |
| | | | | CNN | 0.8136 | 24.7113 | 0.3813 | 47.0739 | 1.0817 | 132 s |
| | | | | LSTM | 0.7211 | 29.8681 | 0.5562 | 40.1199 | 1.2033 | 44 s |

stage with an $R^2p$ of more than 0.9. Fig. 6 shows the best quantitative modelling of FT-IR spectra at the mashing and boiling stages, as well as the correction set and prediction set of predicted values versus true values. It can be seen that their prediction sets all have a very good fitting effect; the real and predicted values basically correspond to the same, and the distribution trend is almost the same; none of them deviates from the samples with too large a distance.

Overall, CARS, combined with LSTM, performs best because the LSTM network can store the data in the internal gating unit, through which the selective transmission of information is realized. Simultaneous quantitative analysis of multiple chemical components by comprehensively analyzing the correlation between chemical components and spectra (Zhu et al., 2022). The variable selection algorithm can better obtain the relevant characteristic information of Plato and total flavonoid substances, thus improving the accuracy and stability of the prediction model. For example, Suleiman A. Haruna et al. explored the potential of combining near-infrared spectroscopy with an efficient variable selection algorithm to quantitatively predict the total flavonoid (TFC) content of raw peanut seeds. The results showed that the Si-CARS-PLS model provided the best fit for total flavonoids ($R^2p = 0.9137$, RPD = 2.49) (Haruna et al., 2023). For both variable input methods, it is easy to see that the full-wavelength input method is not only less accurate but also time-consuming. The advantage of this approach is that it does not require any preprocessing of the spectrum, and the disadvantage is that the design and construction of the network module have some difficulties. The effect of the strategy of CARS combined with LSTM is also demonstrated in Zhao et al. 's study. They combined CARS and LSTM to explore deep features hidden in sensitive wavelengths. They showed that the hybrid depth features of CARS-LSTM can capture complex spectral variations, which can help to improve the relationship between chemical composition and spectral data (R. Zhao et al., 2023).

However, compared to LSTM, CNN did not achieve the desired prediction results. CNN performs moderately well for the quantitative prediction of Plato and a bit poorly for the quantitative prediction of TFC. CNNs can reduce the number of parameters by pooling layers to reduce the data dimensions during network training. However, the pooling layer may cause a loss of internal information and affect the accuracy of the training. Considering multi-layer operations and complex non-linear connections, CNNs are often questioned for their poor interpretability, and neural network-based models have been criticized as black boxes with too little interpretability (Zhang et al., 2020). Therefore, it is hypothesized that the CNN structure designed in this experiment fails to effectively extract the microscopic and macroscopic features hidden in the spectra. Also, the number of samples in the boiling phase is too small, which also prevents the CNN from being adequately and effectively trained (Nallan Chakravartula et al., 2022).

Overall, the accuracy of the best model prediction results still needs to be improved, probably because the spectra are more likely to be affected by the external environment during the acquisition process, such as the light source, the sampling depth, and the position of the fiber optic probe can also cause sampling errors. The experimentally developed model is also only applicable to the prediction of the content of the components of interest using the same brewing process conditions. Applying the CNN model to NIR can merge multiple input channels of different dimensions to give higher performance, and it has higher accuracy performance compared to PLS. However, deep learning models also have their limitations. For example, deep learning requires a large dataset; otherwise, it is easy to overfit. Secondly, the number of parameters used in the model is large, and the process of parameter tuning can be complicated. In addition to this, the hardware requirements are high, and many parameters need to be trained.

## 4. Conclusions

In this study, the Plato and TFC of wort during Qingke beer brewing were analyzed by quantitative modelling using FT-IR, and the best quantitative model for each stage was obtained (Plato-Mashing-CARS-LSTM: $R^2p = 0.9368$, RPD = 2.8582; Plato-Boiling-CARS-LSTM: $R^2p = 0.9398$, RPD = 2.9263; TFC-Mashing-ANN: $R^2p = 0.873$, RPD = 2.0504; TFC-Boiling-CARS-LSTM: $R^2p = 0.9154$, RPD = 2.4842). The changes in

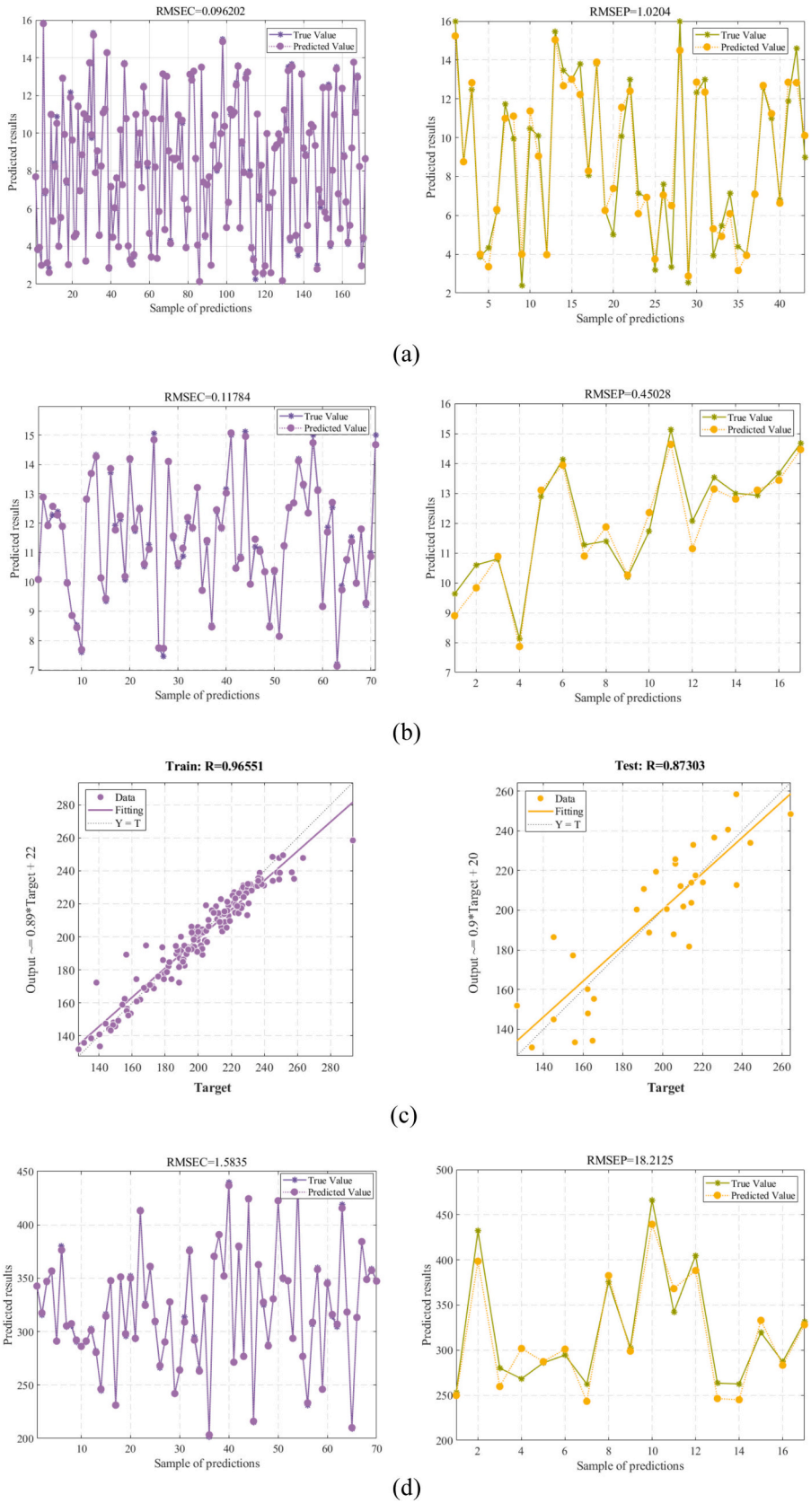


**Fig. 6.** Optimal quantitative prediction model; (a) Correction and prediction sets for Plato-M-CARS-LSTM model; (b) Correction and prediction sets for Plato-B-CARS-LSTM model; (c) Correction and prediction sets for TFC-M-ANN model; (d) Correction and prediction sets for TFC-B-CARS-LSTM model.

Plato and TFC during the mashing and boiling stages of different processes were also analyzed, and the mechanisms and reasons behind them were discussed. This experiment also explored the influence of the variable input method on the prediction effect of the deep learning network model and found that the variable selection algorithm can better extract the characteristic information of the substance, which in turn improves the robustness of the prediction accuracy of the model to adapt to the dynamic change effect, and provides guidance for on-site monitoring and management. By comparing the impact of deep learning methods and traditional machine learning modelling methods, it is demonstrated that deep learning methods have better prediction performance based on a sufficiently large number of samples. The application of deep learning methods to spectral analysis is worthy of recognition. However, there are still some problems and difficulties, such as the best input method of spectral data, the best optimization algorithm of the model, the limitation of the spectral dataset to the functional innovation of the network model structure, and so on, are worthy of more research and exploration. Subsequently, the model will be further optimized, the sample data will be expanded, and the experimental model validation will be carried out, with a view to using the model in the production line for rapid detection of quality control of Qingke beer brewing, and to provide theoretical basis and technical support for the further development of the Deep Learning-Near Infrared online beer brewing process monitoring system.

## CRediT authorship contribution statement

**Xuyan Zong:** Writing – review & editing, Writing – original draft, Supervision, Project administration, Investigation, Funding acquisition, Data curation, Conceptualization. **Xianjiang Zhou:** Writing – original draft, Visualization, Investigation, Formal analysis, Data curation, Conceptualization. **Xinyue Cao:** Visualization. **Shun Gao:** Visualization. **Dongyang Zhang:** Visualization. **Haoran Zhang:** Visualization. **Ran Qiu:** Resources, Formal analysis. **Yi Wang:** Resources, Formal analysis. **Jianhang Wu:** Writing – review & editing, Data curation. **Li Li:** Supervision, Resources, Project administration, Funding acquisition, Formal analysis.

## Declaration of competing interest

The authors declare that they have no known competing financial interests or personal relationships that could have appeared to influence the work reported in this paper.

## Data availability

Data will be made available on request.

## Acknowledgments

This work was supported by Key Lab of Aromatic Plant Resources Exploitation and Utilization in Sichuan Higher Education (23XLY02).

## Appendix A. Supplementary data

Supplementary data to this article can be found online at https://doi.org/10.1016/j.fochx.2024.101673.

## References

Anderson, H. E., Santos, I. C., Hildenbrand, Z. L., & Schug, K. A. (2019). A review of the analytical methods used for beer ingredient and finished product analysis and quality control. *Analytica Chimica Acta, 1085*, 1–20. https://doi.org/10.1016/j.aca.2019.07.061

Aquilani, B., Laureti, T., Poponi, S., & Secondi, L. (2015). Beer choice and consumption determinants when craft beers are tasted: An exploratory study of consumer preferences. *Food Quality and Preference, 41*, 214–224. https://doi.org/10.1016/j.foodqual.2014.12.005

Augusti, R., Fulgêncio, A. C. C., Nogueira, H. M., Gomes, J. C. L., dos Santos, L. B., de Macedo, A. N., & Almeida, M. R. (2024). Enhancing food authentication screening through the integration of chemometrics and ambient ionization mass spectrometry: A comprehensive review. *Trends in Food Science & Technology, 147*. https://doi.org/10.1016/j.tifs.2024.104480

Banerjee, S., Mandal, S., Jesubalan, N. G., Jain, R., & Rathore, A. S. (2024). NIR spectroscopy-CNN-enabled chemometrics for multianalyte monitoring in microbial fermentation. *Biotechnology and Bioengineering*. https://doi.org/10.1002/bit.28681

Coulibaly, W. H., Tohoyessou, Y. M. G., Konan, P. A. K., & Dje, K. M. (2023). Bioactive compounds and antioxidant activities of two industrial beers produced in Ivory Coast. *Heliyon, 9*(8), Article e19168. https://doi.org/10.1016/j.heliyon.2023.e19168

Dong, F., Bi, Y., Hao, J., Liu, S., Yi, W., Yu, W., & Wang, S. (2024). A new comprehensive quantitative index for the assessment of essential amino acid quality in beef using Vis-NIR hyperspectral imaging combined with LSTM. *Food Chemistry, 440*, Article 138040. https://doi.org/10.1016/j.foodchem.2023.138040

Fox, G. (2020). The brewing industry and the opportunities for real-time quality analysis using infrared spectroscopy. *Applied Sciences, 10*(2). https://doi.org/10.3390/app10020616

França, L., Grassi, S., Pimentel, M. F., & Amigo, J. M. (2021). A single model to monitor multistep craft beer manufacturing using near infrared spectroscopy and chemometrics. *Food and Bioproducts Processing, 126*, 95–103. https://doi.org/10.1016/j.fbp.2020.12.011

Fu, X., Yang, B., & Wang, S. (2021). Modeling and control of plasma horizontal displacement for HL-2A tokamak based on LSTM. *Fusion Engineering and Design, 162*. https://doi.org/10.1016/j.fusengdes.2020.112107

Fulgêncio, A. C. D. C., Resende, G. A. P., Teixeira, M. C. F., Botelho, B. G., & Sena, M. M. (2023). Combining portable NIR spectroscopy and multivariate calibration for the determination of ethanol in fermented alcoholic beverages by a multi-product model. *Talanta Open, 7*. https://doi.org/10.1016/j.talo.2023.100180

Giovenzana, V., Beghi, R., & Guidetti, R. (2014). Rapid evaluation of craft beer quality during fermentation process by Vis/NIR spectroscopy. *Journal of Food Engineering, 142*, 80–86. https://doi.org/10.1016/j.jfoodeng.2014.06.017

Haruna, S. A., Li, H., Wei, W., Geng, W., Luo, X., Zareef, M., & Chen, Q. (2023). Simultaneous quantification of total flavonoids and phenolic content in raw peanut seeds via NIR spectroscopy coupled with integrated algorithms. *Spectrochimica Acta. Part A, Molecular and Biomolecular Spectroscopy, 285*, Article 121854. https://doi.org/10.1016/j.saa.2022.121854

Helfer, G. A., Barbosa, J. L. V., Hermes, E., Fagundes, B. J., Santos, R. O., & Costa, A. B. D. (2022). The application of parallel processing in the selection of spectral variables in beer quality control. *Food Chemistry, 367*, Article 130681. https://doi.org/10.1016/j.foodchem.2021.130681

Huang, W., Fan, D., Li, W., Meng, Y., & Liu, T. C.-Y. (2022). Rapid evaluation of milk acidity and identification of milk adulteration by Raman spectroscopy combined with chemometrics analysis. *Vibrational Spectroscopy, 123*. https://doi.org/10.1016/j.vibspec.2022.103440

Jiao, Y., Li, Z., Chen, X., & Fei, S. (2020). Preprocessing methods for near-infrared spectrum calibration. *Journal of Chemometrics, 34*(11). https://doi.org/10.1002/cem.3306

Kourti, T. (2006). The process analytical technology initiative and multivariate process analysis, monitoring and control. *Analytical and Bioanalytical Chemistry, 384*(5), 1043–1048. https://doi.org/10.1007/s00216-006-0303-y

Li, C., Chen, H., Zhang, Y., Hong, S., Ai, W., & Mo, L. (2022). Improvement of NIR prediction ability by dual model optimization in fusion of NSIA and SA methods. *Spectrochimica Acta. Part A, Molecular and Biomolecular Spectroscopy, 276*, Article 121247. https://doi.org/10.1016/j.saa.2022.121247

Li, H., Liang, Y., Xu, Q., & Cao, D. (2009). Key wavelengths screening using competitive adaptive reweighted sampling method for multivariate calibration. *Analytica Chimica Acta, 648*(1), 77–84. https://doi.org/10.1016/j.aca.2009.06.046

Li, L., Sheng, X., Zan, J., Yuan, H., Zong, X., & Jiang, Y. (2023). Monitoring the dynamic change of catechins in black tea drying by using near-infrared spectroscopy and chemometrics. *Journal of Food Composition and Analysis, 119*. https://doi.org/10.1016/j.jfca.2023.105266

Li, L., Zhang, Y., Zheng, J., Li, M., Wang, H., Wu, J., & Zong, X. (2023). Effects of crushing and enzyme treatment on physicochemical, fermentation performance, and antioxidant properties of qingke (hull-less barley) wort. *Lwt, 189*. https://doi.org/10.1016/j.lwt.2023.115545

Lindemann, B., Maschler, B., Sahlab, N., & Weyrich, M. (2021). A survey on anomaly detection for technical systems using LSTM networks. *Computers in Industry, 131*. https://doi.org/10.1016/j.compind.2021.103498

Liu, Y., Liu, Y., Chen, Y., Zhang, Y., Shi, T., Wang, J., & Zhang, Y. (2019). The influence of spectral pretreatment on the selection of representative calibration samples for soil organic matter estimation using Vis-NIR reflectance spectroscopy. *Remote Sensing, 11*(4). https://doi.org/10.3390/rs11040450

Martínez, A., Vegara, S., Herranz-López, M., Martí, N., Valero, M., Micol, V., & Saura, D. (2017). Kinetic changes of polyphenols, anthocyanins and antioxidant capacity in forced aged hibiscus ale beer. *Journal of the Institute of Brewing, 123*(1), 58–65. https://doi.org/10.1002/jib.387

Nallan Chakravartula, S. S., Moscetti, R., Bedini, G., Nardella, M., & Massantini, R. (2022). Use of convolutional neural network (CNN) combined with FT-NIR spectroscopy to predict food adulteration: A case study on coffee. *Food Control, 135*. https://doi.org/10.1016/j.foodcont.2022.108816

Nardini, M., & Garaguso, I. (2020). Characterization of bioactive compounds and antioxidant activity of fruit beers. *Food Chemistry, 305*, Article 125437. https://doi.org/10.1016/j.foodchem.2019.125437

Nobari Moghaddam, H., Tamiji, Z., Akbari Lakeh, M., Khoshayand, M. R., & Haji Mahmoodi, M. (2022). Multivariate analysis of food fraud: A review of NIR based instruments in tandem with chemometrics. *Journal of Food Composition and Analysis, 107*. https://doi.org/10.1016/j.jfca.2021.104343

Rong, D., Wang, H., Ying, Y., Zhang, Z., & Zhang, Y. (2020). Peach variety detection using VIS-NIR spectroscopy and deep learning. *Computers and Electronics in Agriculture, 175*. https://doi.org/10.1016/j.compag.2020.105553

Shao, X., Cui, X., Wang, M., & Cai, W. (2019). High order derivative to investigate the complexity of the near infrared spectra of aqueous solutions. *Spectrochimica Acta. Part A, Molecular and Biomolecular Spectroscopy, 213*, 83–89. https://doi.org/10.1016/j.saa.2019.01.059

Tian, W., Li, Y., Guzman, C., Ibba, M. I., Tilley, M., Wang, D., & He, Z. (2023). Quantification of food bioactives by NIR spectroscopy: Current insights, long-lasting challenges, and future trends. *Journal of Food Composition and Analysis, 124*. https://doi.org/10.1016/j.jfca.2023.105708

Tirado-Kulieva, V. A., Hernandez-Martinez, E., Minchan-Velayarce, H. H., Pasapera-Campos, S. E., & Luque-Vilca, O. M. (2023). A comprehensive review of the benefits of drinking craft beer: Role of phenolic content in health and possible potential of the alcoholic fraction. *Current Research in Food Science, 6*, Article 100477. https://doi.org/10.1016/j.crfs.2023.100477

Xuan, L., Lin, Z., Liang, J., Huang, X., Li, Z., Zhang, X., & Shi, J. (2023). Prediction of resilience and cohesion of deep-fried tofu by ultrasonic detection and LightGBM regression. *Food Control, 154*. https://doi.org/10.1016/j.foodcont.2023.110009

Yan, Z., Liu, H., Li, J., & Wang, Y. (2023). Qualitative and quantitative analysis of Lanmaoa asiatica in different storage years based on FT-NIR combined with chemometrics. *Microchemical Journal, 189*. https://doi.org/10.1016/j.microc.2023.108580

Yin Tan, W., Li, M., Devkota, L., Attenborough, E., & Dhital, S. (2023). Mashing performance as a function of malt particle size in beer production. *Critical Reviews in Food Science and Nutrition, 63*(21), 5372–5387. https://doi.org/10.1080/10408398.2021.2018673

Yu, S., Huan, K., Liu, X., Wang, L., & Cao, X. (2023). Quantitative model of near infrared spectroscopy based on pretreatment combined with parallel convolution neural network. *Infrared Physics & Technology, 132*. https://doi.org/10.1016/j.infrared.2023.104730

Zhang, X., Xu, J., Yang, J., Chen, L., Zhou, H., Liu, X., & Ying, Y. (2020). Understanding the learning mechanism of convolutional neural networks in spectral analysis. *Analytica Chimica Acta, 1119*, 41–51. https://doi.org/10.1016/j.aca.2020.03.055

Zhao, R., An, L., Tang, W., Qiao, L., Wang, N., Li, M., & Liu, G. (2023). Improving chlorophyll content detection to suit maize dynamic growth effects by deep features of hyperspectral data. *Field Crops Research, 297*. https://doi.org/10.1016/j.fcr.2023.108929

Zhao, Y., Liao, P., Chen, L., Zhang, Y., Wang, X., Kang, Q., & Sun, J. (2024). Characterization of the key aroma compounds in a novel Qingke baijiu of Tibet by GC-MS, GC×GC-MS and GC-O-MS. *Food Chemistry Advances, 4*. https://doi.org/10.1016/j.focha.2023.100589

Zhou, X., Li, L., Zheng, J., Wu, J., Wen, L., Huang, M., & Zong, X. (2024). Quantitative analysis of key components in Qingke beer brewing process by multispectral analysis combined with chemometrics. *Food Chemistry, 436*, Article 137739. https://doi.org/10.1016/j.foodchem.2023.137739

Zhu, Z., Qi, G., Lei, Y., Jiang, D., Mazur, N., Liu, Y., & Zhu, W. (2022). A long short-term memory neural network based simultaneous quantitative analysis of multiple tobacco chemical components by near-infrared Hyperspectroscopy images. *Chemosensors, 10*(5). https://doi.org/10.3390/chemosensors10050164

Zong, X., Wu, J., Chen, Z., He, L., Wen, J., & Li, L. (2023). Impact of Qingke (hulless barley) application on antioxidant capacity and flavor compounds of beer. *Journal of Cereal Science, 109*. https://doi.org/10.1016/j.jcs.2022.103624